IDŐJÁRÁS

Quarterly Journal of the Hungarian Meteorological Service
Vol. 115, No. 4, October–December 2011, pp. 275–288

Estimation of structural icing intensity and geometry of aircrafts during different conditions – a fixed-wing approach

Zsolt Bottyán

Aviation Weather Laboratory, Department of Air Traffic Controller and Pilots' Training, Zrínyi Miklós National Defence University, P.O. Box 1, H-5008 Szolnok, Hungary
E-mail: bottyan.zsolt@zmne.hu

(Manuscript received in final form May 8, 2011)

Abstract—The estimation of aircraft structural icing characteristics is a very important procedure as the accreted ice layer may cause some dangerous effects for aircraft such as lift force degradation, increasing of drag force, and malfunction of control surfaces and sensors. The intensity and geometry of ice contamination on the surface of an aircraft depend on meteorological (cloud droplet size distribution, liquid water content, ambient temperature), aerodynamical (airspeed), and geometrical (size and shape of the aircraft) conditions, too. In this paper a 2D similar ice accumulation model is shown which is based on a cylindrical approximation of airfoil and the thermodynamics of icing processes. Applying this model, the intensity and geometry of accreted ice layer can be accessed on the wing of a popular fixed-wing aircraft Cessna -185 Skywagon in a special cold-pool-like weather situation. On the basis of our calculation it is clear, that the severity of icing phenomena strongly depends not only on the meteorological but also on aerodynamical conditions. On the other hand, this method can be adapted for an operational structural airframe icing severity forecasting.

Key-words: aviation meteorology, aircraft structural icing, icing severity, liquid water content, Cessna -185 Skywagon

1. Introduction

The airframe (structural) icing occurs when an aircraft flies mainly under IFR (instrument flight rules) condition (generally in cloud), the ambient static temperature is below zero, and supercooled water droplets impinge and freeze on the aircraft's unprotected surface. The ice accretions cause many dangerous problems during the flight such as reduced lift and increased drag forces,

significantly decreased angle of attack, strong vibrations and structural imbalances of aircrafts, malfunction of control surfaces and air pressure sensors, reduced visibility, and improper radio communication (*Bragg et al.*, 2005). On the other hand, there are some differences between the structural icing of fixed-wing aircrafts and rotorcrafts (helicopters), e.g., the different icing problem of helicopters along their rotor blades (*Gent et al.*, 1987; *Gent et al.*, 2000). On the basis of these facts, a reliable estimation of expected ice accretion during the proposed flight is very useful and important information for the pilots (*Jeck*, 1998; *Fuchs* and *Lütkebohmert*, 2001; *Lankford*, 2001; *Fuchs*, 2003).

Forecasting of airframe (structural) icing of aircrafts is a very complex procedure since the magnitude of the ice accretion on the aircrafts' surfaces highly depends on ambient meteorological and aerodynamical conditions and on aircraft's geometry, too. The rate and amount of structural ice accretion curiously depend on the followings (*Gent et al*., 2000; *Lankford*, 2001; *Bragg et al*., 2005):

- static ambient temperature of airflow around the aircraft,
- static air pressure at the level of flight,
- liquid water content (*LWC*) of cloud,
- cloud droplet size distribution,
- true airspeed (*TAS*) of aircraft, and
- shape and size of aircraft structures with the special regard to wings.

It is clear that the surfaces with high rate of ice accretion are located near the leading edge of wings and tail. They are relatively narrow and their positions are usually opposite the freestream. For that very reason, the ice accretion models have to approach the wing geometry well. In many 2D ice accumulation models a suitable cylinder is applied to describe the ice accretion characteristics along its surface because the cloud droplet trajectory calculation in the airflow around the cylinder is a relatively simple procedure (*List*, 1977; *Lozowski et al*., 1983a; *Makkonen*, 1981; *Launiainen* and *Lyyra*, 1986; *Finstad et al.*, 1988; *Makkonen* and *Stallabrass*, 1987; *Mazin et al*., 2001).

In our work we apply a 2D ice accretion non-rotating cylinder model based on the methods of *Lozowski et al.* (1983a) estimating the rate and geometrical characteristics of ice contamination on a small popular aircraft such as Cessna - 185 Skywagon under different aerodynamic and meteorological conditions.

2. The ice accretion model

The applied ice accretion model is based on the quasi-stationary heat balance equation for a freezing surface which is assumed to define the thermodynamics of icing phenomena, first described by *Ludlam* (1951) and *Messinger* (1953). The local collection efficiency calculation used by *Langmuir* and *Blodgett*

(1946), *Lozowski et al.* (1983a), *Finstad et al.* (1988) and the ice growth estimation along the cylinder surface is described by *Lozowski et al.* (1983a).

Assume a non-rotating horizontal cylinder with a diameter of D_c located in a uniform airstream with the velocity of U (freestream velocity). The streaming air under cloudy circumstances contains supercooled droplets with the concentration of W. Supposing that the airstream and droplets are in thermodynamic and mechanical equilibrium, the temperature of airstream T_a equals the droplet temperature. Apparently, the velocity of supercooled droplets far from the cylinder is also U.

In order to calculate the local impingement of water droplets, we divided the upwind surface of the cylinder into angular sectors of 5º and centered the angles $\theta_i = 5i$º, $i = 1,2,\ldots,18$. The applied droplet size characteristics are also discretized by establishing 9 diameter categories with 5 μm wide intervals centered the diameters $D_j = 5j$ μm, $j = 1,2,\ldots,9$. We assume that the droplets have the same size (central diameter) in each category. On the basis of assumptions mentioned above the local droplet collision efficiency can be calculated for all angular sectors and droplet size categories as follows:

$$\beta_i = \sum_j f_j \beta_{ij}, \tag{1}$$

where f_j is the fraction of total water mass flux in the airflow, containing droplets in the jth diameter category. After that, the liquid water mass flux impinging all sectors along the upstream face of the cylinder can be expressed as:

$$R_{wi} = \beta_i UW. \tag{2}$$

The quasi-stationary heat balance equation for a freezing surface is given by

$$Q_c + Q_e + Q_v + Q_k + Q_f + Q_w + Q_i + Q_r + Q_w^* + Q_f^* = 0, \tag{3}$$

where

– Q_c is the sensible heat flux between freezing surface and airstream;

– Q_e is the latent heat flux of evaporation;

– Q_v is the viscous aerodynamic heating due to airstream;

– Q_k is the flux of kinetic energy of impinged droplets on the icing surface;

– Q_f is the latent heat flux of accretion due to freezing of impinging water;

– Q_w is the sensible heat flux required to warm the freezing water droplets;

– Q_i is the heat flux between the iced and the underlying surface;

– Q_r is the long-wave radiative heat flux;

– Q_w^* is the sensible heat flux required to heat the runback and shedding part of impinging water (similar to Q_w);

– Q_f^* is like Q_f but for runback water only.

If the physical and aerodynamic conditions allow the existence of any unfrozen water on the icing surface (wet-growth ice accretion), the mass of it in any angular sectors is supposed to be moved to the next downstream sector by airstream. On the other hand, we also assume the runback water will be shed into the airstream at $\theta = 90^\circ$. The items in Eq. (3) are formularized as follows:

$$Q_c = h(T_a - T_s), \tag{4}$$

where h is the heat transfer coefficient, T_a and T_s are the temperatures of airstream and icing surface, respectively. The calculation of h is based on the results of *Achenbach* (1977), and we applied the rough cylinder case (because the icing process produces a rough cylinder surface).

The evaporation heat flux term is given by

$$Q_e = h\left(\frac{Pr}{Sc}\right)^{0.63} \frac{\varepsilon l_v}{pc_p}(e_a - e_s), \tag{5}$$

where Pr and Sc are the Prandtl and Schmidt numbers, ε is the ratio of the molecular weights of water vapor and dry air, p is the static pressure of air in the freestream, c_p is the specific heat capacity of dry air at a constant pressure, l_v is the latent heat of vaporization, and finally, e_a and e_s are the saturation water vapor pressures of moist air at T_a and T_s. If the accretion is dry, the latent heat of sublimation l_s has to be applied.

The viscous heating can be given by

$$Q_v = \frac{hr_c U^2}{2c_p}, \tag{6}$$

where r_c is the local recovery factor along the cylinder surface described by *Seban* (1960). This term explains the adiabatic heating due to the air compressibility at higher velocities and the frictional heating in the boundary layer. This factor is very important when the Mach number of airstream is higher than 0.3 (in this case the compressibility of air will be higher than 5%).

The kinetic energy flux of droplets can be calculated by

$$Q_k = \frac{1}{2} R_w U^2, \tag{7}$$

where R_w is the droplet mass flux and $R_w = \beta W U$.

During the freezing of impinging supercooled water the latent heat flux is

$$Q_f = n R_w l_{fs}, \tag{8}$$

where l_{fs} is the latent heat of freezing at T_s and n is the fraction of accreted mass of impinging water. It is obvious, that if $T_s < 273.15$ K then $n = 1$ (dry-growth icing) and in the case of $T_s = 273.15$ K, $n < 1$ (wet-growth icing and there are some runback water along the icy surface of the cylinder).

The sensible heat flux is required to warm the impinging droplets to the equilibrium temperature T_s, and it is given by

$$Q_w = R_w \bar{c}_w (T_a - T_s), \tag{9}$$

where $\bar{c}_w$ is the average specific heat of water between T_a and T_s. Its value is a constant in this model.

The linear approximation of radiative heat flux between the droplets and accreted surface can be written by

$$Q_r = \sigma\left(\varepsilon_a T_a^4 - \varepsilon_s T_s^4\right) = a(T_a - T_s), \tag{10}$$

where ε_a and ε_s are the radiative emissivity of air and surface, respectively, σ is the Stefan-Boltzmann constant, and a is a coefficient.

The amount of existing runback water (unfrozen part of impinged droplets in a given sector) also plays an important role in the heat exchange between the sectors. We suppose, that there are not any parallel flows to the cylinder axis, and the leaving part of runback water (with the steady-state temperature of the given sector) influences the next sector's heat balance only. Obviously the amount of entering runback water adjusts the steady-state temperature in the given sector thus the heat flux in connection with it is described by

$$Q_w^* = R_w^* \bar{c}_w \left(T_s^* - T_s\right), \tag{11}$$

where R_w^* is the mass flux of runback water entering the given sector, T_s^* is the

temperature of runback water. It is obvious the T_s^* equals 0 ºC if there are any runback water (because the steady-state condition). Evidently there is not any runback water into the first sector and the entering part of runback water from the first sector to the second one is the half of the amount of total outflow runback water from the first sector (it is based on the cylinder geometry). The latent heat flux of freezing the runback water is given by

$$Q_f^* = nR_w^* l_{fs}. \tag{12}$$

In our model the Q_i heat flux was omitted and taken into account by Eqs. (4)–(12). In this case, Eq. (3) is a non-linear differential equation which can be solved by numerically within each sector. The two unknowns in Eq. (3) are T_s and n. The solving procedure of Eq. (3) is described by *Gent et al.* (2000) and *Saeed* (2000).

After the calculation of impinging water flux (R_{wi}), runback water flux (R_{wi}^*), and freezing faction (n_i), we can determine the icing flux (R_i) in all sectors:

$$R_i = n_i (R_{wi} + R_{wi}^*). \tag{13}$$

The calculation of the ice growth is given by

$$h_i = \frac{2R_i \delta t / \rho_i}{1 + \left(1 + \frac{4R_i \delta t}{\rho_i D_c} \right)^{0.5}}, \tag{14}$$

where h_i means the local thickness of accretion, δt is the accretion time, and ρ_i is the ice density (*Lozowski et al.*, 1983a). The application of this ice growing approach is limited in time because we have to assume that the ice accretion phenomena does not significantly influence the environment of airstream and the heat exchange around the surface. However, this approach can be applied to estimate the ice accretion rate if we use a short time interval (δt). Experimental results of wind tunnels have confirmed the applicability of Eq. (14) if the time interval is not longer than 5–7 minutes (*Lozowski et al.*, 1983b). On the other hand, the shapes of accreted ice contamination grew during the wind tunnel experiments are very similar to those calculated by the applied ice growth model. These experiments were executed under conditions such as (–5 ºC)–(–15 ºC) temperature, 30.5–122 $\mathrm{m\,s^{-1}}$ airspeed, 0.13–1.27 $\mathrm{g\,m^{-3}}$ *LWC*, and 1–10 minutes time intervals, respectively (*Lozowski et al.*, 1983b).

3. Methods

The ice accretion model described in Section 2 can be used to estimate the amount, rate and, geometry of ice contamination not only along a given cylinder but also along a surface that has the similar curvature (for example, a fixed-wing aircraft airfoil). For the real icing calculation, we applied the twice leading edge radius of the airfoil as cylinder diameter (*Tsao* and *Anderson*, 2005). Our examined fixed-wing aircraft was the popular Cessna -185 Skywagon (*Fig. 1*).

Fig. 1. The examined fixed-wing aircraft: Cessna -185 Skywagon.

The cross section of its wing airfoil (coded by NACA0012) with the 0º angle of attack (AOA) and the corresponding cylinder can be seen in *Fig. 2*. The difference of curvature between the leading edge segment of airfoil and the cylinder is neglectable, so this approximation can be a good choice in our model.

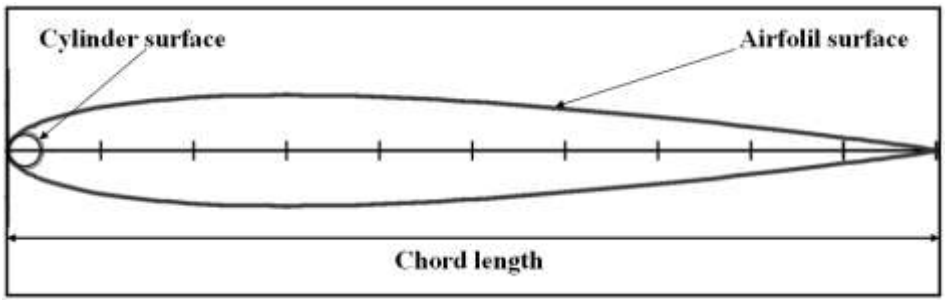

Fig. 2. The cross section of an airfoil and a corresponding cylinder which has the same curvature along the leading edge zone.

The calculation of corresponding cylinder diameter in the case of a given airfoil is based on the method of *Abbott* and *von Doenhoff* (1959):

$$D_c = 2kc, \tag{15}$$

where k is the leading edge radius and the c is the chord length. The data of examined aircraft can be found in *Table 1* (*Lambert*, 1994). As it can be seen, the chord length varies between 1.14 m (wingtip) and 1.63 m (root), so we used 1.385 m as an averaged value, because this number represents the middle segment of wing far enough from the fuselage. Thus, the used leading edge radius of the NACA0012 airfoil was 0.017. Applying Eq. (15) we received the corresponding cylinder diameter value of 0.04709 m. The speed limits of the Cessna -185 aircrafts are 25 m s^{-1} and 80 m s^{-1}, thus, we examined this *TAS* interval in our work (*Table 1*).

Table 1. Some important parameters of the examined fixed-wing aircraft Cessna -185 Skywagon II

Aircraft	Cessna -185 Skywagon II
Wingspan (m)	10.92
Airfoil type	NACA0012
Chord length (m)	1.14 – 1.63
Stall speed (m s^{-1})	25
Maximum speed (m s^{-1})	80
Maximum ceiling (m)	5455

In order to produce real physical (meteorological) background for our examination (as far as possible), we analyzed AIREP icing data between January 1, 2006 and December 31, 2010 over the middle part of Hungary using the atmospheric sounding data of Budapest during this period. There were many icing situations on different air pressure levels, temperatures, and microphysical conditions, and we selected a typical severe icing event of January 14, 2006 which was in connection with thick low level stratiform clouds under a strong inversion layer (cold-pool-like weather situation over the Carpathian Basin) (*Table 2*).

Table 2. AIREP reports during icing situations of January 14, 2006. The icing phenomenon is signed by bold underlined setting

Date and time	**AIREP text**
12:57:26 UTC, January 14, 2006	**SEV ICING** BTN GRD AND 2000FT ON 31R FINAL BY B737
15:28:58 UTC January 14, 2006	**SEV ICING** BTN GRD AND 5000FT ON 13R FINAL BY B737
18:56:52 UTC January 14, 2006	**SEV ICING** BTN 5000FT AND GROUND ON FINAL 13R

As it can be seen, the icing zones were located between the ground and 2000 ft (600 m) and later 5000 ft (1500 m) on January 14, 2006 (*Fig. 3*). We have to note that severe icing for a Boeing -737 does not mean the same icing severity occurrence for other aircrafts!

Based on the mentioned data, our examined air temperature values were –3 ºC, –5 ºC, and –7 ºC, and air pressure values 1010, 970, and 890 hPa, respectively (*Fig. 3*).

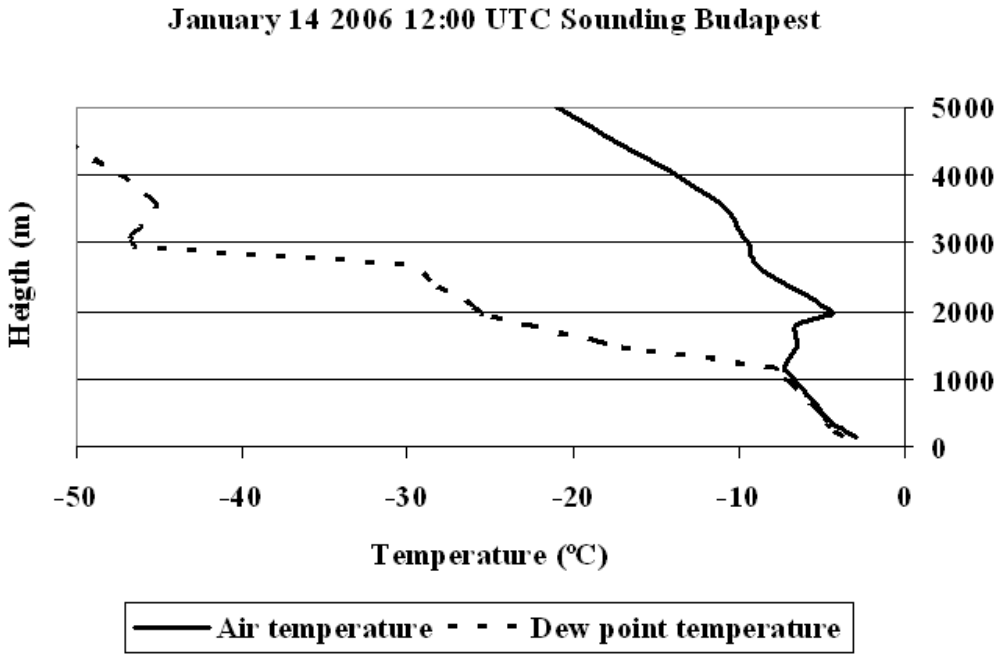

Fig. 3. Vertical air temperature and dew point temperature profiles of January 14, 2006 during AIREP based icing phenomena.

Taking into account the given cloud structure in which the icing was detected by some aircrafts on the mentioned day, we supposed a typical cloud water droplet size distribution (Γ-distribution, *Geresdi*, 2004) with 20 μm median volume diameter (*MVD*), and we also assumed that this distribution was constant in the cloud. On the other hand, the used (presumed) liquid water content (*LWC)* values were 0.2 g kg^{-1} and 0.5 g kg^{-1} in our calculation. The applied values of cloud droplet size distribution and *LWC* in the thick low stratus are in tune with the measurements of *Kunkel* (1971), the work of *Jeck* (2002), and the numerical simulation of *Geresdi* and *Rasmussen* (2005).

We also supposed a 5 minutes hypothetical flight time of our aircraft under selected meteorological condition, because this time interval is not longer than used in the experimentally tested ice accretion model (*Lozowski et al.*, 1983b).

4. Results and discussion

First of all, we calculated the ice accumulation and its rate along the airfoil (cylinder) surface under the given meteorological conditions at 12 UTC on January 14, 2006 over Budapest. Our results – regarding the ice growth intensity values – are in *Table 3*. The *TAS* (tone airspeed of aircraft) as well as the *U*

(freestream velocity) were 60 m s^{-1} and the applied icing severity categories were the international standards by *Jeck* (1998), which are similar to ICAO ones. In spite of the same icing intensity category (moderate), it can be seen that the maximum icing growth intensity values vary between 0.436 and 1.249 mm min^{-1}. The largest value is three times higher than the smallest one, so the moderate marking of icing severity is not always enough to sign this phenomenon exactly. Obviously the higher values can be found at higher *LWC*, because the amounts of impinging droplets are proportional to *LWC* values.

Table 3. The calculated maximum ice growth intensity and severity under different meteorological conditions at 12 UTC on January 14, 2006 over Budapest

Temperature (ºC)	**Pressure (hPa)**	**LWC (g kg^{-1})**	**Ice growth intensity (mm min^{-1})**	**Icing severity**
–3	1010	0.0002	0.51	Moderate
–3	1010	0.0005	1.25	Moderate
–5	970	0.0002	0.44	Moderate
–5	970	0.0005	1.20	Moderate
–7	890	0.0002	0.44	Moderate
–7	890	0.0005	1.17	Moderate

Supposing that the *LWC* was a constant value of 0.0005 g kg^{-1}, the aircraft flew at the 970 hPa pressure level, and the ambient temperature was –5 ºC we were able to estimate the icing intensities with different *TAS* values, too.

Our results can be seen in *Table 4*. Under conditions from 30 m s^{-1} to 60 m s^{-1} *TAS* values,the maximum icing rate is moderate, but if the aircraft reaches 70 m s^{-1} *TAS* value the icing rate is severe! We examined the *TAS* values when the icing rate changes from moderate to severe and from light to moderate. In the examined case the moderate/severe limit *TAS* value is 64 m s^{-1}, and the light/moderate one is 28 m s^{-1}. Allowing for Cessna -185 speed limits (*Table 1*), we can establish light (25–27 m s^{-1}), moderate (28–63 m s^{-1}) or severe (64–80 m s^{-1}) icing situations as a function of speed of flight during the same meteorological conditions! The thickness of accreted ice layer varies between 1.75 mm and 8.25 mm after 5 minutes flight time, thus, the amount of ice layer may reach the dangerous thickness (near maximum *TAS*) during a short time period (within 15 minutes).

However, the estimated ice growth intensity is not enough to predict the exact icing risk potential for a given aircraft, because the spatial distribution of the ice layer has a crucial effect in the disturbance of airflow around the wing (*Bragg et al*., 2005). While the icing process is dry-growth (n =1), the geometry of accreted ice layer mainly elliptical with its maximum ice growth at the leading edge, supposing 0º AOA (at the stagnation point or leading edge) (*Lozowski*, 1983a; *Tsao* and *Anderson*, 2005). On the other hand, if the icing process is already wet-growth, the unfrozen part of the collided droplets begin to

move from the leading edge along the airfoil's surface and it may freeze at the farther part of the wing causing the dangerous horn-shaped ice accretion instead of the elliptical one (*Fig. 4*).

Table 4. Icing severity conditions of Cessna -185 aircraft as a function of *TAS* under given constant meteorological conditions (T_a = –5 °C; p = 970 hPa; LWC = 0.0005 g kg^{-1})

TAS (m s^{-1})	**Icing growth intensity (mm min^{-1})**	**Thickness of ice layer after 5 minutes flight (mm)**	**Icing severity**
25	0.35	1.75	Light
30	0.48	2.41	Moderate
40	0.72	3.60	Moderate
50	0.95	4.76	Moderate
60	1.18	5.92	Moderate
70	1.41	7.07	Severe
80	1.65	8.25	Severe

The fundamental problems of an aircraft which has a similar horn-shaped ice contamination on its wing during flight are the extremely high drag force and mainly the loss of lift force because of the appearance of strongly turbulent airflow behind the big ice horns (between the ice horn and the airflow trajectory reattachment zone) (*Fig. 4*). This lift force degradation may reach the 30 – 40% of the clear (non-contaminated) value (*Cooper et al*., 1984; *Bragg et al*., 2005).

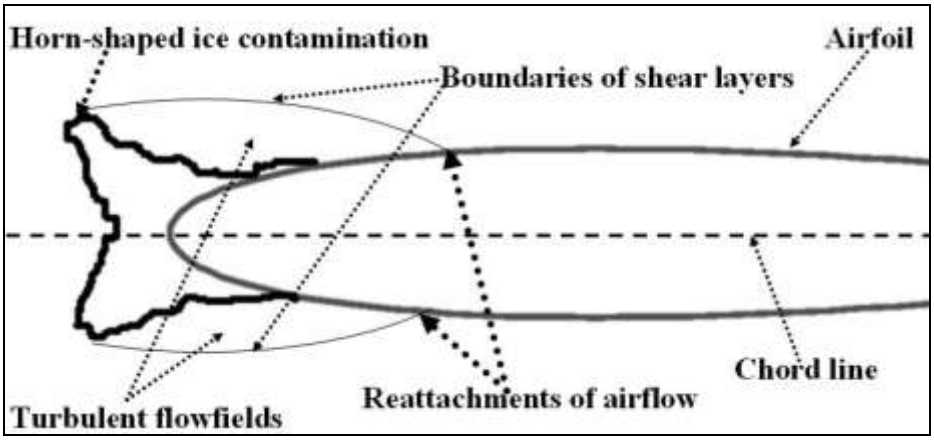

Fig. 4. The geometry of horn-shaped ice contamination and its effect on the airflow around NACA0012 airfoil.

It is clear that the correct estimation of accreted ice layer under different meteorological conditions requires the prediction of geometry of contaminated surface, too. In our work, we described a 2D estimation of the structural icing geometry of a given type of aircraft under measured (T_a, p) and supposed (LWC, U, and droplet size distribution) ambient conditions as it can be seen in *Fig. 5*.

There are some important notes associated with the two calculated cases:

- At higher air temperature (T_a = –3 ºC, near 0 ºC), the ice envelopes have horn-like shape and this form is more significant at higher speed (*TAS* (*U*) = 50 and 80 m s^{-1}). It is caused by the large amount of runback water (wet-growth icing) moving along the airfoil surface and freezing farther from the stagnation point (leading edge) (*Fig. 5*, right).

- At maximum airspeed (*TAS* (*U*) = 80 m s^{-1}), we can see the horn-shaped ice contamination around the cylinder (airfoil) in both cases, but the distance of the location of maximum accretion from the stagnation point and the maximum of accreted ice thickness are different. When T_a= –7 ºC (*Fig. 5*, left), the amount of runback water is smaller, thus, the ice horn is also thinner and its position is closer to the stagnation point (leading edge) than in the other case (T_a = –3 ºC).

- When the airspeed is close to the minimum value of Cessna-185 (*TAS* = 25 m s^{-1}), the ice accretion geometry has the elliptical form in both cases, because the icing is dry-growth yet. It is clear that this shape causes less significant anomalies in airflow around the wing than the horn-iced one (*Fig. 5*, right and left).

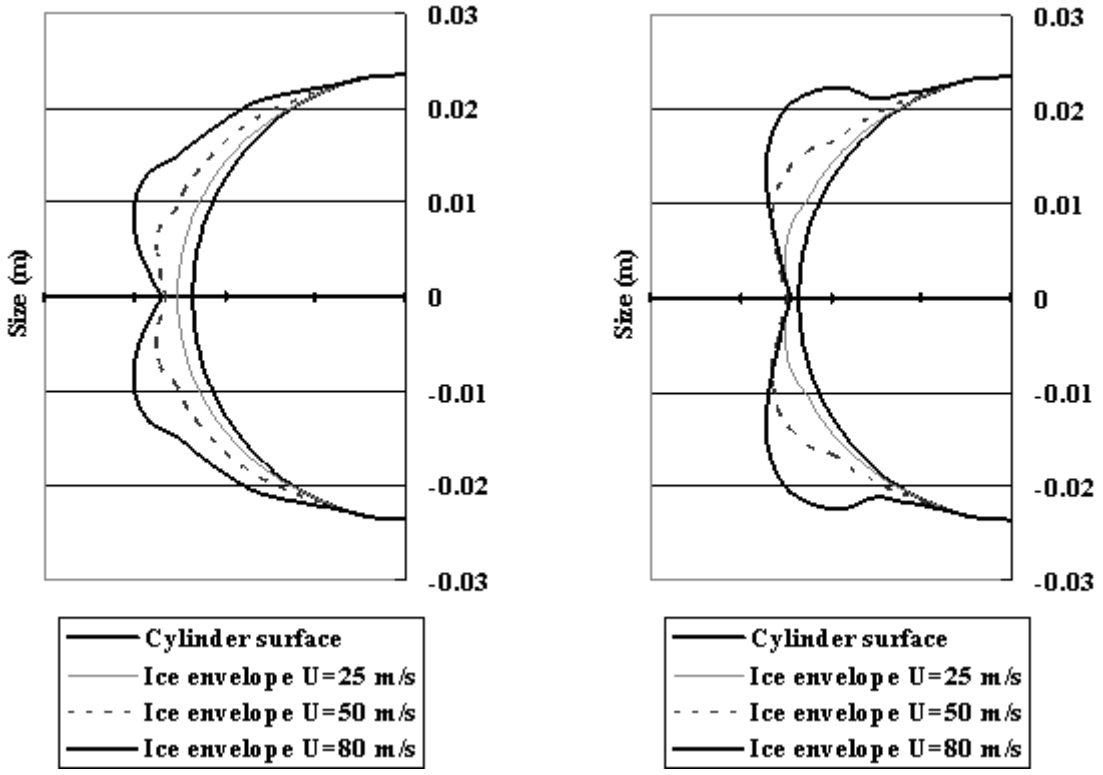

Fig. 5. The 2D geometry of computed accreted ice layers on the surface of the given cylinder (airfoil) after 5 minutes flight time. Left: T_a= –7 ºC; p = 890 hPa; *LWC* = 0.0005 g kg^{-1}; Right: T_a= –3ºC; p = 1010 hPa; *LWC* = 0.0005 g kg^{-1}.

As long as the geometrical effects are initially constants, the environmental parameters may vary along wide ranges during the flight. It follows that the provision of a responsible quasi real-time prediction in the matters of rate, amount, and geometry of airframe ice accretion requires the good knowledge of meteorological (cloud microphysical) conditions and flight plan (airspeed, duration, and 3D route of flight), together. On the other hand, the necessary high resolution values of signed meteorological variables can be produced by a meso-scale numerical weather model such as WRF with a corresponding parameterization or a coupled microphysical model (*Skamarock et al.*, 2005; *Geresdi et al.*, 2001; *Rasmussen* and *Geresdi*, 2005).

Finally, we have to note that further additional studies are necessary to generate the corresponding high resolution meteorological fields of the mentioned ambient physical variables for operational use of our ice accretion model.

5. Summary

On the basis of the described model and our results, we are able to estimate the concrete icing rate and geometry on the wings of a given fixed-wing aircraft during a relatively short time period. There is also a good advantage to calculate the correct limits of the icing severities regarding to given meteorological, aerodynamical and geometrical conditions (aircraft-dependent estimations).

Applying the calculated geometry (shape) of the accreted ice layer, we are able to predict the most dangerous horn-iced phenomena and its probable location within the cloud.

The effectively accreted ice characteristics highly depend on flight time as well. Knowing the flight environment, we may derive a maximum flight time for a given fixed-wing aircraft during this situation without any dangerous icing (flight path optimization).

Moreover, the embedding of a similar ice accretion model (such as described one) into an operative forecasting procedure can level up the usage and reliability of icing predictions and may lead to higher level of flight safety.

***Acknowledgements*—**The author thanks *István Geresdi* and *Ferenc Wantuch* for useful suggestions and comments on work, *Péter Szalóky* and *Péter Kardos* for providing AIRMET data set.

References

Abbott, I. H. and *von Doenhoff, A.E.*, 1959: *Theor. Wing Sections*. Dover, New York.

Achenbach, E., 1977: The effect of surface roughness on the heat transfer from circular cylinders to the cross flow of air. *Int. J. Heat Mass Transfer 20*, 359-369.

Bragg, M.B., Broeren, A.P. and *Blumenthal, L.A.*, 2005: Iced-airfoil aerodynamics. *Prog. Aerospace Sci. 41*, 323-362.

Cooper, W.A., Sand, W.R., Politovich, M.K. and *Veal, D.L.*, 1984: Effects of Icing on Performance of a Research Aircraft. *J. Aircraft 21*, 708-715.

Finstad, J.K., Lozowski, E.P. and *Gates, E.M.*, 1988: A computational investigation of water droplet trajectories. *J. Atmos. Ocean. Tech. 5*, 160-170.

Fuchs, W., 2003: Forecast of aircraft icing by use of boundary layer model products: First experiences. *Proceedings of The 13th International Offshore and Polar Engineering Conference*. Honolulu, USA, 423-428.

Fuchs, W. and *Lütkebohmert, M.,* 2001: Aircraft icing forecast. *Proceedings of The 11th International Offshore and Polar Engineering Conference*. Stavanger, Norway, 686-689.

Gent, R.W., Markiewicz, R.H. and *Cansdale, J.T.*, 1987: Further studies of helicopter rotor ice accretion and protection. *Vertica 11*, 473-492.

Gent, R.W., Dart, N.P. and *Cansdale, J.T.*, 2000: Aircraft icing. *Phil. Trans. Roy. Soc. London. A. 358*, 2873-2911.

Geresdi, I., 2004: *Cloudphysics* (in Hungarian). Dialóg Campus Kiadó. Budapest – Pécs.

Geresdi, I. and *Rasmussen, R.M.*, 2005: Freezing drizzle formation in stably Stratified layer clouds: The role of giant nuclei and aerosol particle size distribution and solubility. *J. Atmos. Sci. 62*, 2037-2067.

Geresdi, I. Rasmussen, R.M., Thompson, G., Manning, K., and *Karplus, E.*, 2001: Freezing drizzle formation in stably stratified layer clouds: The role of radiative cooling of cloud droplets, cloud condensation nuclei, and ice initiation. *J. Atmos. Sci. 59*, 837-860.

Jeck, R., 1998: A workable, aircraft-specific icing severity scheme. Appendix A. *Preprints of AIAA-98-0094. 36th Aerospace Sciences Meeting and Exhibit*. Reno, USA, 1-12.

Jeck, R., 2002: Icing Design Envelopes (14 CFR Parts 25 and 29, Appendix C) Converted to a Distance-Based Format. *Final Report of U.S. Department of Transportation Federal Aviation Administration Office of Aviation Research*. Washington, USA, 1-48.

Kunkel, B.A., 1971: Fog drop-size distributions measured with a laser hologram camera. *J. Appl. Meteorol. 10*, 482-486.

Lambert, M. (ed.), 1994: *Jane's All theWorld's Aircrafts*. Jane's Publishing Co., London, UK.

Langmuir, I. and *Blodgett, K.B.*,1946: A mathematical investigation of water droplet trajectories. *Collected Works of Irving Langmuir*. 10. Pergamon Press, 348-393.

Lankford, T.T., 2001: *Aviation Weather Handbook*. McGraw-Hill, New York.

Launiainen, J. and *Lyyra, M.*, 1986: Icing on a non-rotating cylinder under conditions of high liquid water content in the air: II. Heat transfer and rate of ice growth. *J. Glaciol. 32*, 12-19.

List, R., 1977: Ice acretions on structures. *J. Glaciol. 19*, 451-465.

Lozowski, E.P., Stallabrass, J.R., and *Hearty, P.F.*, 1983a: The icing of an unheated nonrotating cylinder. Part I: A simulation model. *J. Clim. Appl. Meteorol. 22*, 2053-2062.

Lozowski, E.P., Stallabrass, J.R., and *Hearty, P.F.*, 1983b: The icing of an unheated nonrotating cylinder. Part II: Icing wind tunnel experiments. *J. Clim. Appl. Meteorol. 22*, 2063-2074.

Ludlam, F.H., 1951: The heat economy of a rimed cylinder. *Q. J. Roy. Meteor. Soc. 77*, 663-666.

Makkonen, L., 1981: Estimating intensity of atmospheric ice accretion on stationary structures. *J. Appl. Meteorol. 20*, 595-600.

Makkonen, L. and *Stallabrass, J.R.*, 1987: Experiments on the cloud droplet collision efficiency of cylinders. *J. Clim. Appl. Meteorol. 26*, 1406-1411.

Mazin, I.P., Korolev, A.V., Heymsfield, A., Isaac, G.A. and *Cober, S.G.*, 2001: Thermodynamics of icing cylinder for measurements of liquid water content in supercooled clouds. *J. Atmos. Ocean. Tech. 18*, 543-558.

Messinger, B.L., 1953: Equilibrium temperature of an unheated icing surface as a function of airspeed. *J. Aeronaut. Sci. 20*, 29-41.

Rasmussen, R.M., and *Geresdi, I.* 2005: Freezing drizzle formation in stably stratified layer clouds. Part II: The role of giant nuclei and aerosol particle size distribution and solubility. *J. Atmos. Sci. 62*, 2037-2057.

Saeed, F., 2000: State-of-the-art aircraft icing and anti-icing simulation. *ARA J. 25-27*, 106-113.

Seban, R.A., 1960: The influence of free stream turbulence on the local heat transfer from cylinders. *J. Heat Trans. 82*, 101-107.

Skamarock, W.C., Klemp, J.B., Dudhia, J., Gill, D.O., Barker, D.M., Wang, W. and *Powers, J.G.*, 2005: A *Description of the Advanced Research WRF Version 2*. NCAR Technical. Note, Boulder, USA, 1-88.

Tsao J-C., and *Anderson, D.N.*, 2005: Additional study of water droplet median volume diameter (MVD) effects on ice shape. *NASA/CR-2005-213853 report*, 1-11.